



**Novel Blue Fluorescent Emitters structured by Linking
Triphenylamine and Anthracene Derivatives for Organic
Light-Emitting Devices with EQE exceeding 5%**

Journal:	<i>Journal of Materials Chemistry C</i>
Manuscript ID	TC-ART-05-2019-002773.R1
Article Type:	Paper
Date Submitted by the Author:	20-Jul-2019
Complete List of Authors:	Zhang, Jing; Key Laboratory of Interface Science and Engineering in Advanced Materials, Ministry of Education, Taiyuan University of Technology Zhao, Yaping; Taiyuan University of Technology Xu, Huixia; 2. Shanxi Research Center of Advanced Materials Science and Technology, Zhang , Di; Taiyuan University of Technology Miao, Yanqin; 1. Key Laboratory of Interface Science and Engineering in Advanced Materials, Ministry of Education, Taiyuan University of Technology, Shinar, Ruth; Iowa State University, Shinar, Joseph; Iowa State University, Physics & Astronomy Wang, Hua; 2. Shanxi Research Center of Advanced Materials Science and Technology, Xu, Bingshe; Taiyuan University of Technology Wu, Yucheng; Taiyuan University of Technology

ARTICLE

Novel Blue Fluorescent Emitters structured by Linking Triphenylamine and Anthracene Derivatives for Organic Light-Emitting Devices with EQE exceeding 5%

Received 00th January 20xx,
Accepted 00th January 20xx

DOI: 10.1039/x0xx00000x

Jing Zhang^a, Yaping Zhao^a, Huixia Xu^{a*}, Di Zhang^a, Yanqin Miao^{a*}, Ruth Shinar^b, Joseph Shinar^c, Hua Wang^a, Bingshe Xu^a, Yucheng Wu^a

Achieving an external quantum efficiency exceeding 5% for traditional blue fluorescent organic light emitting devices (OLEDs) is still a current challenge due to a 25% limit of radiative exciton yield. Bipolar organic molecules with the special hybrid local-excited and charge-transfer state have exhibited huge potential to address this issue. Herein, we designed and synthesized two novel bipolar compounds, namely **TPA-AN-NA** and **TPA-AN-TFP**, which were structured by simply linking a donor of triphenylamine (TPA) and both acceptors of anthracene derivatives. Both resulting compounds show good blue emission with the emission peaks of 468 and 471 nm and photoluminescent quantum yields of 30.68 and 23.96% in thin films for **TPA-AN-NA** and **TPA-AN-TFP**, respectively. They also exhibit good solubility and can dissolve in several organic solvents with different polarities. Further, the fabricated blue OLEDs with **TPA-AN-NA** and **TPA-AN-TFP** as emitters also well realize corresponding blue emission with electroluminescent peaks at 464 and 472 nm, respectively. The **TPA-AN-NA**-based blue device achieves high external quantum efficiency of 5.44% and radiative exciton yield of 56.68%, exceeding the theoretical limit.

Introduction

Organic light-emitting devices (OLEDs) are widely considered as the next generation display and potential lighting technologies due to their unique attributes of high colour contrast, efficiency, light weight, and special flexibility.¹⁻³ Emitting materials are the prerequisite for developing high performance OLEDs. Tremendous efforts have been made for obtaining high performance emitting materials with high quantum yield, good colour purity, and long-term stability. However, compared with the long-band emitting materials (green and red), the blue ones are still very rare due to their intrinsic large energy gap, poor thermal stability, and low photoluminescent quantum yield (Φ_{PL}),⁴⁻⁷ which becomes a bottleneck for the development of OLEDs. Typically, in traditional blue fluorescent OLEDs, only 25% single excitons can emit radiatively, while 75% triplet excitons decay non-radiatively.^{8, 9} The external quantum efficiency (EQE) in fluorescent OLEDs is limited to only 5%, which isn't beneficial for developing high efficiency OLEDs.¹⁰⁻¹² Therefore, an effective way to boost device efficiency of blue OLEDs is to enable contribution of non-emissive triplet excitons to light emission,

consequently, breaking the limitation of 25% radiative exciton yield (η_r).

The donor-acceptor (D-A)-type bipolar organic molecules with special excited states have displayed the tremendous potential to address the above-mentioned issue.^{13, 14} Generally, the charge-transfer (CT) excited state in D-A molecules with the weak bonding energy of the exciton facilitates efficient reverse intersystem-crossing (RISC) from triplet to singlet to improve η_r .¹⁵⁻¹⁷ Simultaneously, the locally excited (LE) state with a high oscillator strength can enhance Φ_{PL} owing to the overlap of the highest occupied molecular orbital (HOMO) and lowest unoccupied molecular orbital (LUMO).¹⁸ This unique hybrid local excited and charge-transfer (HLCT) excited state in D-A molecules can simultaneously contribute to high η_r and high Φ_{PL} , consequently improving the electroluminescent efficiency of blue fluorescent OLEDs.¹⁹⁻²¹

In order to construct the efficient blue-light emitting materials with HLCT state, the donor and acceptor units should be carefully selected to regulate the LE and CT excited states. Additionally, to avoid the long-band emission, neither the strong donor nor acceptor should be chosen.¹⁰ Triphenylamine (TPA) is a medium electron-donating group with an unique space propeller structure with large steric hindrance, which can effectively reduce the exciton binding energy and favour the formation of a CT state.²²⁻²⁴ Anthracene (An) is an weak electron-withdrawing group with its planar conjugated structure, which will promote the overlap between HOMO and LUMO and improve the LE state.²⁵⁻²⁹

^a Key Laboratory of Interface Science and Engineering in Advanced Materials, Ministry of Education, Taiyuan University of Technology, Taiyuan 030024, China.
*E-mails: xuhuixia@tyut.edu.cn; miaoyanqin@tyut.edu.cn

^b Microelectronics Research Center and Electrical & Computer Engineering Department, Iowa State University, Ames, IA 50011, USA.

^c Ames Laboratory, USDOE and Physics & Astronomy Department, Iowa State University, Ames, IA 50011, USA.

†Electronic Supplementary Information (ESI) available.

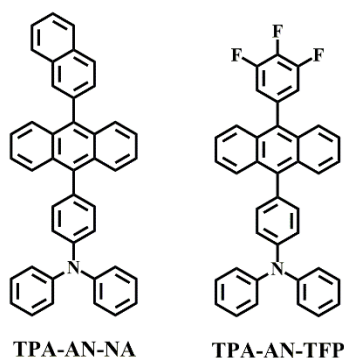


Fig. 1 Molecular structures of **TPA-AN-NA** and **TPA-AN-TFP**.

Herein, two novel bipolar compounds were synthesized by simply linking a donor of TPA and both acceptors of anthracene derivatives, namely **TPA-AN-NA** and **TPA-AN-TFP**, respectively. The molecular structures of two blue emitters are shown in Fig. 1. As expected, two resulting compounds show good blue emission with the emission peaks of 468 and 471 nm and photoluminescent quantum yields of 30.68 and 23.96 % for **TPA-AN-NA** and **TPA-AN-TFP** in thin films, respectively. And the fabricated OLED with **TPA-AN-NA** and **TPA-AN-TFP** as emitters also well realize corresponding blue emission with EL peak at 464 and 472 nm, respectively. Moreover, the **TPA-AN-NA**-based blue device achieves excellent electroluminescent performance with the maximum current efficiency (CE), power efficiency (PE), and external quantum efficiency (EQE) reaching 7.16 cd/A, 6.09 lm/W, 5.44 %, respectively, where the EQE is obviously higher than the reported limit of 5%. These results demonstrate that the TPA- and An-based emitters have a promising application in blue OLEDs.

Results and discussion

Structure characteristics

The synthetic routes and molecular structures of **TPA-AN-NA** and **TPA-AN-TFP** are depicted in Scheme S1 and Fig. 1. The intermediate compound 1 and two target products were prepared through the palladium catalysed Suzuki coupling reaction, and then purified by column chromatography on silica gel. The chemical structures of the compounds were confirmed by ^1H NMR and ^{13}C NMR, as shown in ESI. There are large torsion angles of 68° between TPA and adjacent phenyl and 72° between the anthracene and phenyl ring in compound **TPA-AN-NA** (Fig. 2). When electron-withdrawing 3,4,5-trifluorophenyl is introduced in compound **TPA-AN-TFP**, the two torsion angles are increased to 85° and 90° , respectively. The

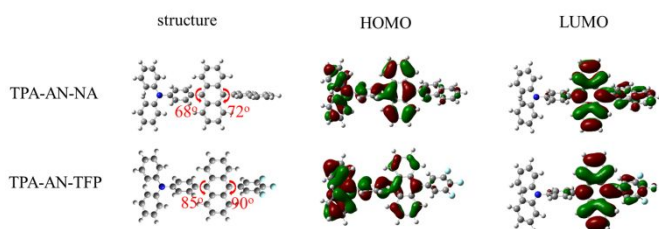


Fig. 2 Optimized structure and spatial distribution of the HOMO and LUMO orbitals of **TPA-AN-NA** and **TPA-AN-TFP**.

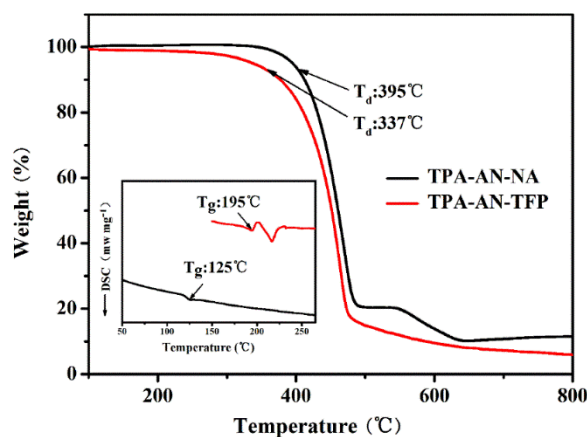


Fig. 3 TGA and DSC (insert) curves of **TPA-AN-NA** and **TPA-AN-TFP**.

conjugation effect between anthracene and trifluorophenyl was completely suppressed. The comparison showed that both the compounds exhibited similar LUMO distributions, which are mainly located at the anthracene moieties (Fig. 2). The HOMO of **TPA-AN-NA** was mostly populated on the anthracene and extended to TPA unit, and a little contribution from naphthalene, while the HOMO of **TPA-AN-TFP** was largely contributed to TPA group and anthracene.

The thermal stabilities were investigated by TGA and DSC under a nitrogen atmosphere. As presented in Fig. 3 and Table 1, compounds **TPA-AN-NA** and **TPA-AN-TFP** exhibit high decomposition temperatures (T_d , corresponding to 5% weight loss) of 395 and 337 $^\circ\text{C}$, respectively, and high T_g s of 125 and 195 $^\circ\text{C}$ due to the rigid structure of anthracene unit. These results suggest that the two compounds possess good thermal and morphological stabilities, which are important for applications in organic electronic devices.

Photophysical properties

The UV-vis absorption and emission spectra in CH_2Cl_2 solution and neat film of **TPA-AN-NA** and **TPA-AN-TFP** at room temperature are shown in Fig. 4. The relevant data are also summarized in Table 1. The absorption peaks below 300 nm are attributed to the π - π^* transitions of benzene rings. While, the longer wavelength band absorptions appear in the range of 300-400 nm, characteristic of

the π - π^* transitions from anthracene and TPA. The absorption

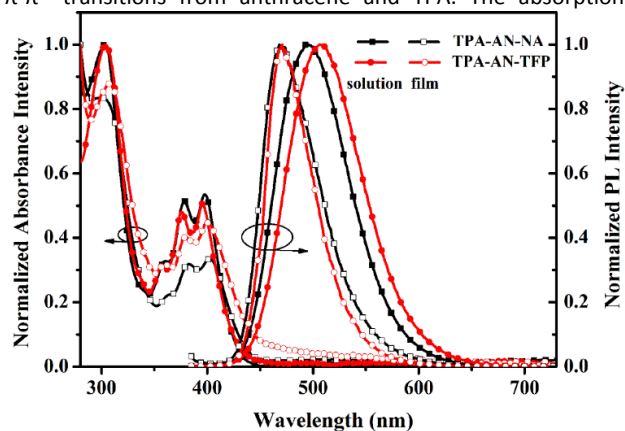


Fig. 4 The UV-vis absorption and emission spectra in CH_2Cl_2 solution and neat film at room temperature of **TPA-AN-NA** and **TPA-AN-TFP**.

spectra of **TPA-AN-NA** and **TPA-AN-TFP** displayed the similar patterns, suggesting that the electron-withdrawing 3,4,5-trifluorophenyl has no effect on the ground state.

The maximum emission peaks of **TPA-AN-NA** and **TPA-AN-TFP** in CH_2Cl_2 solution were observed at 495 and 506 nm, respectively. Compared with **TPA-AN-NA**, the emission of **TPA-AN-TFP** displayed a redshift of 11 nm due to the introduction of the electron-withdrawing F atoms. It is noteworthy that the emission peaks of **TPA-AN-NA** and **TPA-AN-TFP** in films exhibit large blue-shifts of ~ 27 and ~ 35 nm relative to that in CH_2Cl_2 solution, located at 468 nm and 471 nm, respectively, which is attributed to the large dihedral angle between anthracene and TPA.

The optical band-gap (E_g) of **TPA-AN-NA** and **TPA-AN-TFP** were calculated to be 2.86 and 2.83 eV, respectively, from the intersection between the absorption and emission spectra in films. The cyclic voltammograms of **TPA-AN-NA** and **TPA-AN-TFP** are presented in Fig. 5. The HOMO level (E_{HOMO}) was calculated according to the equation (1)

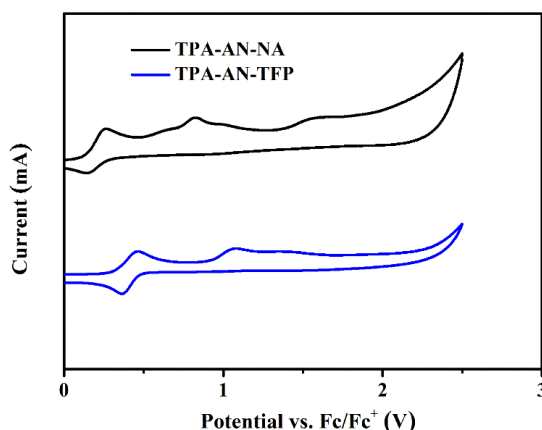


Fig. 5 Cyclic voltammograms of **TPA-AN-NA** and **TPA-AN-TFP** in CH_2Cl_2 solution.

$$E_{\text{HOMO}} = -4.8 - e(E_{\text{c}}^{\text{ox}} - E_{\text{f}}^{\text{ox}}) \text{V} \quad (1)$$

where E_{c}^{ox} is the first oxidation peak measured from the CV curve and E_{f}^{ox} is the oxidation peak of ferrocene. The LUMO level (E_{LUMO}) was calculated from the equation (2)

$$E_{\text{LUMO}} = E_{\text{HOMO}} + E_g \quad (2)$$

Both **TPA-AN-NA** and **TPA-AN-TFP** have almost the same HOMO levels (-5.37 and -5.41 eV) due to the same donor of TPA. The LUMO level of -2.58 eV for compound **TPA-AN-TFP** is lower than that of -2.51 eV for **TPA-AN-NA** because of the electron-withdrawing ability of 3,4,5-trifluorophenyl.

Solvatochromic effect

To understand the nature of the excited states, the absorption (Fig. S3 ESI*) and emission (Fig. 6) spectra of **TPA-AN-NA** and **TPA-AN-TFP** were examined in different solvents. The absorption spectra were insensitive to the solvent polarity, suggesting the low dipole potential in ground state. Unlike the absorption spectra, the emission of **TPA-AN-NA** and **TPA-AN-TFP** showed obvious solvatochromic effect. As the solvent polarity increasing from the low-polarity hexane to the high-polarity dimethyl sulfoxide (DMSO), the emission peaks of **TPA-AN-NA** and **TPA-AN-TFP** exhibited redshifts of 92 and 104 nm, respectively, which correspond to the remarkable CT-state characteristic. The emission of **TPA-AN-TFP** demonstrates a relatively large red-shift due to the strong CT-state character from TPA to trifluorophenyl and anthracene. The Lippert-Mataga model was applied in the estimation of the excited state dipole moments with the increase of solvent polarity³⁰. The two compounds exhibited two section linear relations ($0.0012 \leq f \leq 0.1$ and $0.2 \leq f \leq 0.305$), as shown in Fig. S4 (ESI*), corresponding to the LE state with the small slope in low-polarity solvents ($0.0012 \leq f \leq 0.1$) and CT state with a large slope in high-polarity solvents ($0.2 \leq f \leq 0.305$). In moderate-polarity solvents ($0.1 \leq f \leq 0.2$), such as chloroform and ethyl ether, they may possess a hybridized local and charge transfer (HLCT) state. The μ_{e} values of **TPA-AN-NA** and **TPA-AN-TFP** were estimated to be 3.73 and 7.63 D in low-polarity solvents and increased to 21.72 and 24.72 D in the high-polarity solvents, respectively. Therefore, they possess the LE excited state ($\mu_{\text{e}} < 10$ D) in low-polarity solvents and dominant-CT state ($\mu_{\text{e}} > 20$ D) in high-polarity solvents according to HLCT theory³¹.

The transient decay curves in different solvents and thin films were measured (Fig. S5, S6; Table S1 and S2, ESI*). With increasing of polarities, the lifetimes increased with single exponential,

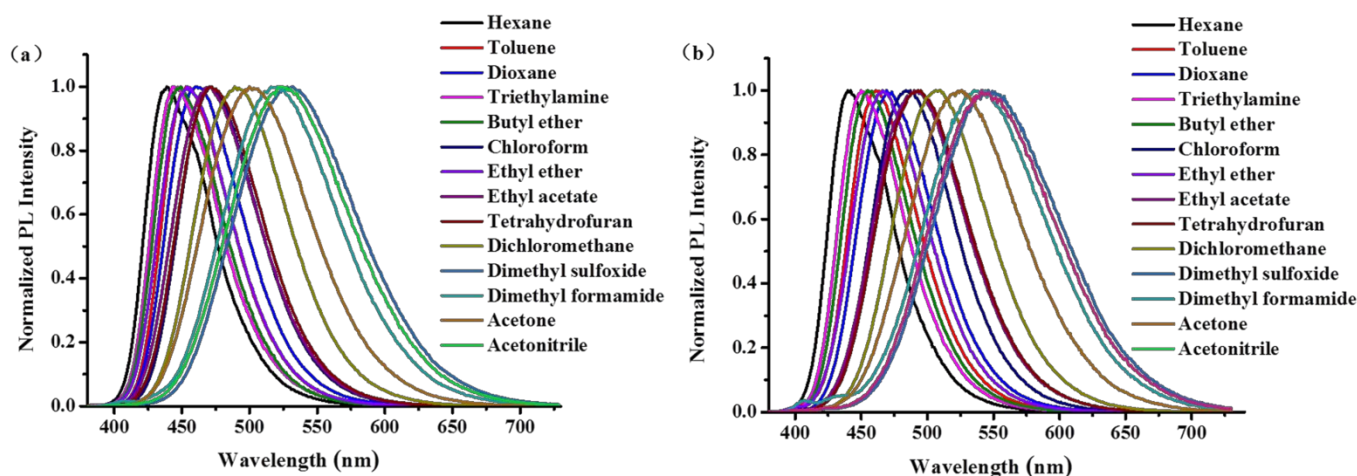


Fig. 6 the emission spectra of **TPA-AN-NA** (a) and **TPA-AN-TFP** (b) in different solvents.

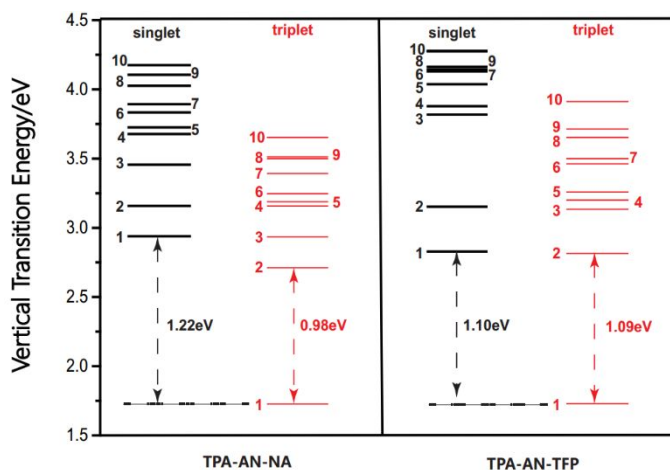
Table 1 The photophysical, electrochemical and thermal properties of TPA-AN-NA and TPA-AN-TFP

Compound	λ_{abs}^a (nm)	λ_{em}^a (nm)	λ_{abs}^b (nm)	λ_{em}^b (nm)	E_g^c (eV)	HOMO/LUMO (eV)	Φ_{PL}^d (%)	T_d/T_g^e (°C)
TPA-AN-NA	360,378,398	495	362,383,402	468	2.86	-5.37/-2.51	30.68	395/125
TPA-AN-TFP	355,375,395	506	360,379,400	471	2.83	-5.41/-2.58	23.96	337/195

^a) Measured in CH₂Cl₂ solution; ^b) Measured in the neat film; ^c) Obtained from the intersection of absorption and emission spectra; ^d) Quantum yield (Φ_{PL}) from the pure film; ^e) From TGA and DSC measurements.

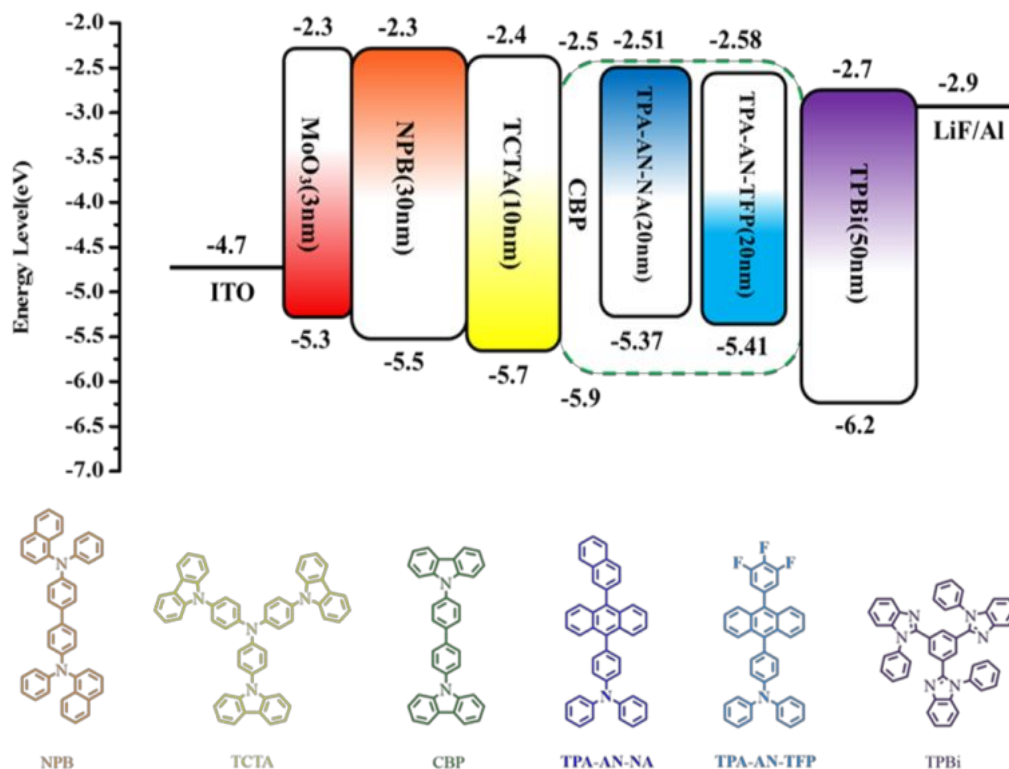
indicating that there was a reverse from LE to CT state. The transient PL spectra in moderate-polarity solvents (Ethyl ether, Tetrahydrofuran) can be well fitted to a single exponential decay in Table S1 and S2 (ESI*), revealing the HLCT feature of the excited state.³²

To further verify the HLCT characteristic of both compounds, the excited states were calculated by the TD-DFT. For TPA-AN-NA, the hole and particle of S₁ showed spatial separation and partly orbital overlap (Fig. S7, ESI*). The separation section facilitated the CT state, and the certain orbital overlap led to the a LE state, indicating the formation of HLCT components. On the other hand, the S₁ of TPA-AN-TFP displayed CT due to the completely separate hole and particle. The low-lying triplet state T₁ of two materials were LE state because their hole and particle were almost completely overlapped. The high-lying T₃ of TPA-AN-NA and T₂ of TPA-AN-TFP possess obvious HLCT states. The energy gaps of the S₁ and T₁ of TPA-AN-NA and TPA-AN-TFP reached 1.22 and 1.10 eV, and therefore, the RISC process from the T₁ to S₁ state by TADF were prevented (Fig 7). For TPA-AN-NA, the singlet–triplet energy splitting between S₁ and T₃ states of 0.004 eV enable a more competitive RISC from T₃ to S₁. The similar process was occurred between S₁ and T₂ for TPA-AN-TFP due to the small energy gap of 0.02 eV. Therefore, the RISC of two

**Fig. 7** Excited state (singlet and triplet) energy diagram of TPA-AN-NA and TPA-AN-TFP.

compounds can be achieved by “hot exciton” process, which the triplet exciton originated from high-lying state T₃ and T₂, respectively.

Electroluminescence performance

**Scheme 1** Energy-level diagram and molecular structures of all materials used in devices.

The above characterization analysis indicates **TPA-AN-NA** and **TPA-AN-TFP** as blue emitters have the potentials applied in the development of high-performance blue OLEDs. In order to evaluate EL characteristic of **TPA-AN-NA** and **TPA-AN-TFP**, firstly, the non-doped devices with **TPA-AN-NA** and **TPA-AN-TFP** as emitters were fabricated, and device structure was follow as: ITO/MoO₃ (3 nm)/NPB (30 nm)/TCTA (10 nm)/ **TPA-AN-NA** or **TPA-AN-TFP** (20 nm)/TPBi (50 nm)/LiF (1 nm)/Al (100 nm). In these devices, ITO and Al are used as the anode and cathode, respectively; MoO₃ and LiF are acted as the hole and electron injection layers, respectively; N, N'-di(1-naphthyl)-N, N'-diphenyl-(1,1'-biphenyl)-4,4'-diamine (NPB) and tris(4-carazoyl-9-ylphenyl)amine (TCTA) are served as hole-transport layer and electron blocking layer respectively; and 1,3,5-tris(N-phenylbenzi-midazole-2-yl)benzene (TPBi) was used as the electron-transport layer. The molecular structure of organic materials involved in OLED fabrication and device structure and energy level diagrams is shown in Scheme 1.

Fig. 8 reveals the EL spectra, current density-voltage-luminance (*J-V-L*), current efficiency-current density-power efficiency (*CE-J-PE*), and external quantum efficiency-luminance (*EQE-L*) characteristic curves of **TPA-AN-NA** and **TPA-AN-TFP**-based non-doped devices, where the key performance parameters are also listed in Table 2. Two non-doped devices all realize blue emission with peaks located

at 464 nm and 472 nm and corresponding to CIE coordinates of (0.14, 0.16) and (0.15, 0.24) for **TPA-AN-NA** and **TPA-AN-TFP**-based devices, respectively. Clearly, their EL spectra are similar to their PL spectra in thin films, indicate the EL emissions well originate from two emitting materials themselves. The EL spectra for two devices have no changes at various voltages from 4 to 9 V, as shown in Fig. S8 and S9 (ESI*), exhibiting extremely high stability. From Fig. 8(b), the **TPA-AN-NA**-based device shows a low turn-on voltage of 3.0 V, which is lower than that for the **TPA-AN-TFP**-based devices, which can be ascribed to a smaller energy barrier between **TPA-AN-NA** and functional layers. And two devices obtain high luminance of 8344 and 9899 cd/m² for **TPA-AN-NA** and **TPA-AN-TFP**-based device respectively. In addition, two devices also achieve excellent device efficiency with the maximum CE, PE, EQE of 6.37 cd/A, 6.68 lm/W, and 4.93% for **TPA-AN-NA**-based device and 4.91 cd/A, 3.33 lm/W, and 2.77% for **TPA-AN-TFP**-based device. The higher efficiency for **TPA-AN-NA**-based device is owing to a higher fluorescence quantum yield than that of **TPA-AN-TFP**-based in the film state.

Considering the influence of aggregation effect for emitters, both **TPA-AN-NA** and **TPA-AN-TFP** are doped in 4,4'-bis(N-carbazoyl)-1,1'-biphenyl (CBP) to fabricate two doped devices with the structure of ITO/MoO₃ (3 nm)/NPB (30 nm)/TCTA (10 nm)/CBP: 20 wt% **TPA-AN-NA** or **TPA-AN-TFP** (20 nm)/TPBi (50 nm)/LiF (1 nm)/Al

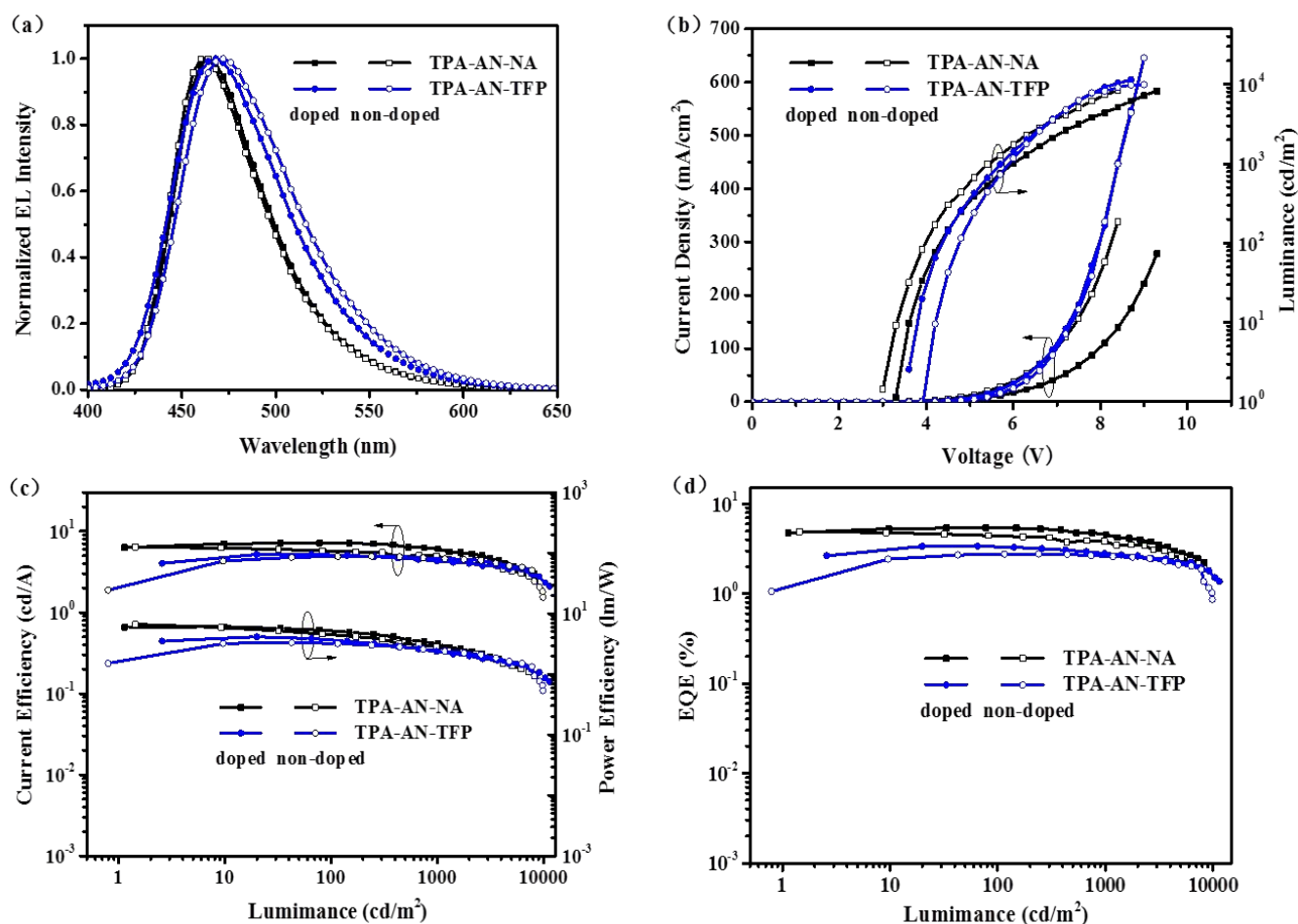


Fig. 8 (a) EL spectra under driven voltage of 8 V; (b) *J-V-L* curve; (c) *CE-L-PE* curve and (d) *EQE-L* curve for non-doped and doped blue devices based on **TPA-AN-NA** and **TPA-AN-TFP**.

Table 2 EL performance of devices based **TPA-AN-NA** and **TPA-AN-TFP**

Emitter	λ_{max} (nm)	V_{on}^a (V)	L_{max} (cd/m ²)	CE_{max} (cd/A)	PE_{max} (lm/W)	EQE_{max} (%)	CIE (x, y)
TPA-AN-NA	464	3.0	8344	6.37	6.68	4.93	(0.14, 0.16)
CBP: TPA-AN-NA	460	3.3	8246	7.16	6.09	5.44	(0.14, 0.16)
TPA-AN-TFP	472	3.9	9899	4.91	3.33	2.77	(0.15, 0.24)
CBP: TPA-AN-TFP	468	3.6	11450	5.17	4.16+	3.38	(0.14, 0.20)

^a Turn-on voltage estimated at a brightness of 1 cd/m²

(100 nm). As seen in Fig. 8 (a), similar to the non-doped devices, the doped devices also realize good blue emission with peaks at 460 and 468 nm. But the doped devices achieve higher EL performance, for example, the maximum luminance, CE, PE, and EQE are up to 8246 cd/m², 7.16 cd/A, 6.09 lm/W, and 5.44% for **TPA-AN-NA**-based doped device and 11450 cd/m², 5.17 cd/A, 4.16 lm/W, and 3.38% for **TPA-AN-TFP**-based doped device, respectively. For higher device performance, it is likely attributed to a reduced exciton quenching in doped devices. The radiative exciton utilization (η_r) for all devices can be calculated by the Equation (3)

$$EQE = \gamma \times \Phi_{PL} \times \eta_r \times \eta_{out} \quad (3)$$

where γ is the carrier recombination efficiency, which is assumed to be 100%; Φ_{PL} is the PL quantum yield of emitters.³³ The Φ_{PL} s of **TPA-AN-NA** and **TPA-AN-TFP** in non-doped films were measured to be 30.68 and 23.96%, and 48.07 and 34.72% when doped in CBP films, respectively; η_r is the radiative exciton yield and η_{out} is the light out-coupling efficiency, which is generally considered to be 20%. Calculated η_r in **TPA-AN-NA** and **TPA-AN-TFP**-based non-doped devices are 80.35 and 57.80% respectively. While η_r in the doped devices are 56.58 and 48.68%. These values of radiative exciton yields have broken the limitation of 25% for the fluorescent OLEDs, indicating that there was the effective up-conversion process from some triplet excitons to singlet ones in these devices.

Generally, the high η_r and RISC in fluorescent devices can be achieved by three mechanisms: thermally activated delayed fluorescence (TADF)³⁴, triplet-triplet annihilation (TTA)³⁵, and the formation of an HLCT excited state. The transient PL spectra of **TPA-AN-NA** in film and THF solution show only the single exponential decay with lifetimes of 3.42 and 2.31 ns, respectively (Fig. S6 and Table S1, ESI*). For **TPA-AN-TFP**, the lifetimes in THF solution and film are 5.20 and 2.12 ns (Table S2 ESI*), respectively. No delayed lifetimes in the range of μ s were observed. Furthermore, the correlations between the luminance and current density of all devices are linear^{36,37} (Fig. S10, ESI*). These results indicate that the high η_r values do not result from TADF or TTA processes. Hence, HLCT excited states are mainly responsible for the high radiative utilization from triplets.

Conclusions

In this work, two novel blue fluorescent materials of **TPA-AN-NA** and **TPA-AN-TFP** were designed and synthesized by linking a donor of triphenylamine (TPA) and both acceptors of anthracene derivatives. Both synthesized compounds show hybrid local-excited and charge-transfer state. The resulting OLEDs with **TPA-AN-NA** and **TPA-AN-TFP** as emitters exhibit the blue emission with electroluminescent peaks at 464 and 472 nm with the CIE coordinates of (0.14, 0.16) and (0.15, 0.24), respectively. In addition, the **TPA-AN-NA**-based blue device achieves high external quantum efficiency exceeding the theoretical limit 5% in fluorescent blue OLEDs, reaching 5.44%. The achievement for high singlet exciton-utilizing efficiencies of 80.35 and 56.58% is resulting from the formation the HLCT excited states.

Experimental section

Materials and methods

All the reagents and solvents used for the syntheses and measurements were purchased from commercial suppliers and were used without further purification unless otherwise noted. ¹H NMR and ¹³C NMR spectra were measured with a Switzerland Bruker DR × 600. UV-vis absorption spectra were measured using Lambda Bio 40. The Photoluminescence (PL) spectra were recorded using HORIBA FluoroMax-4 spectrophotometer. The absolute quantum yields were determined through an absolute method employing an integrating sphere. Thermogravimetric analysis (TGA) curves were undertaken using a Netzsch TG 209F3 under a dry nitrogen atmosphere heating from room temperature up to 800 °C at a rate of 10 °C/min. Differential scanning calorimetry (DSC) was performed on a DSC Q2000 at a heating rate of 10 °C/min from 40 to 300 °C, then cooling down to room temperature rapidly, and heating up to 300 °C at a heating rate of 10 °C/min again; the melting temperature (T_m) was obtained from the first heating scan and the glass transition temperature (T_g) was determined from the second heating scan. Cyclic voltammetry (CV) was carried out in a solution of tetrabutylammonium perchlorate (0.1 M) in acetonitrile at a scan rate of 100 mV/s at room temperature using a conventional three electrode cell, which consisted of the working electrode platinum plate, the counter electrode platinum wire, and the reference electrode calomel electrode.

DFT calculation

Theoretical calculations were performed using the Gaussian 03 package. Geometry optimization was performed by density functional theory (DFT) in B3LYP/6-31G(d) basis sets.

OLED fabrication and characterization

The OLEDs with area of $3 \times 3 \text{ mm}^2$ were fabricated by vacuum deposition onto the indium tin oxide (ITO) glass substrates. The substrates were cleaned, in the following order, with deionized water, acetone, and ethanol. The electroluminescence (EL) spectra and CIE coordinates were measured by a PR-655 spectrophotometer. The current density-voltage-luminance (*J-V-L*) characteristics of the OLEDs were recorded using Keithley 2400 Source Meter and ST-900M Spot Brightness Meter.

Synthesis of TPA-AN-NA and TPA-AN-TFP

Synthesis of 4-(10-(naphthalen-2-yl)anthracen-9-yl)-N,N-diphenylaniline (TPA-AN-NA)

A mixture of 4-bromo-N,N-diphenylaniline (0.973 g, 3 mmol), 9,9-diphenyl-9,10-(10-(naphthalen-2-yl)anthracen-9-yl)boronic acid (1.15 g, 3.3 mmol), Pd(PPh₃)₄ (0.173 g, 0.15 mmol) and K₂CO₃ (2.0 M aqueous solution, 10.0 mL) were dissolved in 30 mL of 1,2-dimethoxyethane, and then heated to reflux for 12 h. After cooling to room temperature, the solution was extracted with dichloromethane. The organic material was dried by anhydrous MgSO₄ and concentrated. Then crude product was purified by silica gel chromatography. The desired product was obtained as yellow powder (1 g, yield: 63%). Purity can be reached 96%. ¹H NMR (600 MHz, DMSO, δ): 8.19 (d, *J* = 8.7 Hz, 1H), 8.12 (d, *J* = 7.8 Hz, 1H), 8.05-8.01 (m, 2H), 7.77 (dd, *J* = 5.4, 4.3 Hz, 2H), 7.67-7.59 (m, 5H), 7.48 (td, *J* = 8.8, 6.4, 1.3 Hz, 2H), 7.43-7.38 (m, 8H), 7.25-7.22 (m, 6H), 7.13 (td, *J* = 7.4, 1.1 Hz, 2H). ¹³C NMR (151 MHz, CDCl₃, δ): 146.01, 145.38, 135.32, 134.88, 131.62, 130.89, 130.32, 128.36, 127.76, 127.56, 126.26, 126.08, 125.24, 124.57, 124.36, 123.20, 122.88, 121.40.

Synthesis of N, N-diphenyl-4-(10-(3,4,5-trifluorophenyl)anthracen-9-yl)aniline (TPA-AN-TFP)

9-bromo-10-(3,4,5-trifluorophenyl)anthracene (1) and N,N-diphenyl-4-(10-(3,4,5-trifluorophenyl)anthracen-9-yl)aniline (TPA-AN-TFP) were prepared with a similar procedure as that of TPA-AN-NA. The desired product was obtained as yellow-green powder (0.6 g, yield: 60%). Purity is 98%. ¹H NMR (600 MHz, CDCl₃, δ): 7.88-7.84 (m, 2H), 7.64-7.59 (m, 2H), 7.42-7.39 (m, 4H), 7.34 (t, *J* = 7.9 Hz, 4H), 7.30-7.25 (m, 8H), 7.10 (dt, *J* = 18.2, 7.1 Hz, 4H). ¹³C NMR (151 MHz, CDCl₃, δ): 150.68, 150.31, 141.23, 136.01, 134.93, 132.94, 132.59, 132.33, 130.28, 128.78, 128.06, 127.71, 126.14, 125.87, 118.58.

Conflicts of interest

There are no conflicts to declare.

Acknowledgements

Ames Laboratory is operated by Iowa State University for the US Department of Energy under Contract No. DE-AC02-07CH11358. This

work was financially supported by National Natural Scientific Foundation of China (61705156, 21071108, 60976018, 61605138, 61775155), Shanxi Provincial Key Innovative Research Team in Science and Technology (201513002-10). We also thank professor Runfeng Chen in Nanjing University of Posts and Telecommunications for calculation data.

References

1. C. W. Tang and S. A. VanSlyke, *Appl. Phys. Lett.*, 1987, **51**, 913-915.
2. P. Tao, Y. Miao, Y. Zhang, K. Wang, H. Li, L. Li, X. Li, T. Yang, Q. Zhao, H. Wang, S. Liu, X. Zhou, B. Xu, W. Huang, *Org. Electron.*, 2017, **45**, 293-301.
3. J.-H. Jou, S. Kumar, A. Agrawal, T.-H. Li and S. Sahoo, *J. Mater. Chem. C*, 2015, **3**, 2974-3002.
4. P. Tao, Y. Zhang, J. Wang, L. Wei, H. Li, X. Li, Q. Zhao, X. Zhang, S. Liu, H. Wang, W. Huang, *J. Mater. Chem. C*, 2017, **5**, 9306-9314.
5. S. Wang, M. Qiao, Z. Ye, D. Dou, M. Chen, Y. Peng, Y. Shi, X. Yang, L. Cui, J. Li, C. Li, B. Wei, and W.-Y. Wong, *iScience*, 2018, **9**, 532-541
6. Y. Feng, P. Li, X. Zhuang, K. Ye, T. Peng, Y. Liu and Y. Wang, *Chem. Commun.*, 2015, **51**, 12544-12547.
7. K. S. Yook and J. Y. Lee, *Adv. Mater.*, 2012, **24**, 3169-3190.
8. J. R. Sheats, H. Antoniadis, M. Hueschen, W. Leonard, J. Miller, R. Moon, D. Roitman and A. Stocking, *Science*, 1996, **273**, 884-888.
9. M. A. Baldo, D. F. O'Brien, M. E. Thompson and S. R. Forrest, *Phys. Rev. B*, 1999, **60**, 14422-14428.
10. Q. Zhang, J. Li, K. Shizu, S. Huang, S. Hirata, H. Miyazaki and C. Adachi, *J. Am. Chem. Soc.*, 2012, **134**, 14706-14709.
11. S. Chen, J. Lian, W. Wang, Y. Jiang, X. Wang, S. Chen, P. Zeng and Z. Peng, *J. Mater. Chem. C*, 2018, **6**, 9363-9373.
12. C.-L. Ho and W.-Y. Wong, *New J. Chem.* 2013, **37**, 1665-1683
13. S. Zhang, W. Li, L. Yao, Y. Pan, F. Shen, R. Xiao, B. Yang and Y. Ma, *Chem. Commun.*, 2013, **49**, 11302-11304.
14. W. Li, Y. Pan, R. Xiao, Q. Peng, S. Zhang, D. Ma, F. Li, F. Shen, Y. Wang, B. Yang and Y. Ma, *Adv. Funct. Mater.*, 2014, **24**, 1609-1614.
15. L. Yao, S. Zhang, R. Wang, W. Li, F. Shen, B. Yang and Y. Ma, *Angew. Chem. Int. Ed. Engl.*, 2014, **53**, 2119-2123.
16. X. Liang, Z. Wang, L. Wang, M. Hanif, D. Hu, S. Su, Z. Xie, G. Yu, Y. Bing and Y. Ma, *Chin. J. Chem.*, 2017, **35**, 1559-1568.
17. Y. Yu, L. Ma, X. Yang, H. Zhou, H. Qin, J. Song, G. Zhou, D. Wang and Z. Wu, *Adv. Optical Mater.*, 2018, **6**, 1800060-1800071.
18. B. Liu, Z.-W. Yu, D. He, Z.-L. Zhu, J. Zheng, Y.-D. Yu, W.-F. Xie, Q.-X. Tong and C.-S. Lee, *J. Mater. Chem. C*, 2017, **5**, 5402-5410.
19. J. Shi, L. Xu, C. Chen, X. Lv, Q. Ding, W. Li, S. Xue and W. Yang, *Dyes Pigments*, 2019, **160**, 962-970.
20. S. Liu, X. Zhang, C. Ou, S. Wang, X. Yang, X. Zhou, B. Mi, D. Cao and Z. Gao, *ACS Appl. Mater. Interfaces*, 2017, **9**, 26242-26251.
21. J. Jiang, D. Hu, M. Hanif, X. Li, S. Su, Z. Xie, L. Liu, S. Zhang, B. Yang and Y. Ma, *Adv. Optical Mater.*, 2016, **4**, 2109-2118.
22. Y. Zhi, B. Zhao, R. Cao, Y. Xu, J. Wang, D. Dang, C. Gao and L. Meng, *Dyes Pigments*, 2018, **153**, 291-299.
23. H. Yu, H. Liu, H. Tan, H. Yao, Y. Song, S. Zhu, N. Song, B. Zhang and S. Guan, *Dyes Pigments*, 2018, **158**, 97-103.

ARTICLE

Journal Name

24. R. Braveenth, I.-J. Bae, Y. Wang, S. Kim, M. Kim and K. Chai, *Appl. Sci.*, 2018, **8**, 1168.
25. A. M. Thangthong, D. Meunmart, N. Prachumrak, S. Jungsuttiwong, T. Keawin, T. Sudyoadsuk and V. Promarak, *Tetrahedron*, 2012, **68**, 1853-1861.
26. J. Huang, J. H. Su, X. Li, M. K. Lam, K. M. Fung, H. H. Fan, K. W. Cheah, C. H. Chen and H. Tian, *J. Mater. Chem.*, 2011, **21**, 2957-2964.
27. Z.-Y. Xia, Z.-Y. Zhang, J.-H. Su, Q. Zhang, K.-M. Fung, M.-K. Lam, K.-F. Li, W.-Y. Wong, K.-W. Cheah, H. Tian and C. H. Chen, *J. Mater. Chem.*, 2010, **20**, 3768-3774.
28. L. Wang, Z.-Y. Wu, W.-Y. Wong, K.-W. Cheah, H. Huang and C. H. Chen, *Org. Electron.*, 2011, **12**, 595-601.
29. D. Zhang, X. Song, H. Li, M. Cai, Z. Bin, T. Huang and L. Duan, *Adv. Mater.*, 2018, **30**, 1707590.
30. Z. R. Grabowski, R. Krystyna and R. Wolfgang, *Cheminform*, 2003, **34**, 3899-4032.
31. Q. Wan, B. Zhang, J. Tong, Y. Li, H. Wu, H. Zhang, Z. Wang, Y. Pan, B. Z. Tang, *Phys. Chem. Chem. Phys.*, 2019, **21**, 9837-9844
32. W. Li, D. Liu, F. Shen, D. Ma, Z. Wang, T. Feng, Y. Xu, B. Yang and Y. Ma, *Adv. Funct. Mater.*, 2012, **22**, 2797-2803.
33. S. Zhang, L. Yao, Q. Peng, W. Li, Y. Pan, R. Xiao, Y. Gao, C. Gu, Z. Wang, P. Lu, F. Li, S. Su, B. Yang and Y. Ma, *Adv. Funct. Mater.*, 2015, **25**, 1755-1762.
34. H. Uoyama, K. Goushi, K. Shizu, H. Nomura and C. Adachi, *Nature*, 2012, **492**, 234-238.
35. D. Chen, G. Xie, X. Cai, M. Liu, Y. Cao and S. J. Su, *Adv. Mater.*, 2016, **28**, 239-244.
36. P. Y. Chou, H. H. Chou, Y. H. Chen, T. H. Su, C. Y. Liao, H. W. Lin, W. C. Lin, H. Y. Yen, I. C. Chen and C. H. Cheng, *Chem. Commun.*, 2014, **50**, 6869-6871.
37. C. Ganzorig and M. Fujihira, *Appl. Phys. Lett.*, 2002, **81**, 3137-3139.

TOC Figure

Novel Blue Fluorescent Emitters structured by Linking Triphenylamine and Anthracene Derivatives for Organic Light-Emitting Devices with EQE exceeding 5%

we designed and synthesized two novel bipolar compounds, namely **TPA-AN-NA** and **TPA-AN-TFP** by simply linking a donor of triphenylamine and both acceptors of anthracene derivatives. The **TPA-AN-NA**-based blue device achieves high external quantum efficiency of 5.44% and radiative exciton yield of 56.68%, exceeding the theoretical limit.

